JOINT EUROPEAN TORUS

JET–P(91)48

H.P. Summers, M. von Hellermann, P. Breger, J. Frieling, L.D. Horton,
R. Konig, W. Mandl, H. Morsi, R. Wolf, F. de Heer, R. Hoekstra,
W. Fritsch and JET Team

Atomic Processes Relevant to Neutral Beam Based Tokamak Diagnostics

Atomic Processes Relevant to Neutral Beam Based Tokamak Diagnostics

H.P. Summers, M. von Hellermann, P. Breger, J. Frieling, L.D. Horton,
R. Konig, W. Mandl, H. Morsi, R. Wolf, F. de Heer[1], R. Hoekstra[1],
W. Fritsch[2] and JET Team*

JET-Joint Undertaking, Culham Science Centre, OX14 3DB, Abingdon, UK

[1]FOM-AMOLF, Groningen, Netherlands.
[1]Hahn-Meitner Institute, Berlin, Germany
** See Appendix 1*

Preprint of an Invited Paper presented to APS Topical Meeting on
Atomic Processes in Plasmas, Portland, Maine, USA., 26th August 1991

ATOMIC PROCESSES RELEVANT TO NEUTRAL BEAM BASED TOKAMAK DIAGNOSTICS

H.P. Summers, M. von Hellermann, P. Breger, J. Frieling, L.D. Horton,
R. Konig, W. Mandl, H Morsi, R. Wolf
JET Joint Undertaking, Abingdon, Oxon., OX14 3EA, U.K.

F. de Heer, R. Hoekstra
FOM-AMOLF, 1009 DB Amsterdam & KVI, 9747 AA Groningen, Netherlands

W. Fritsch
Hahn-Meitner Institute, Glienicker Strasse 100, Berlin, Germany

ABSTRACT

Charge exchange and beam emission spectroscopy in magnetic confinement fusion plasmas are reviewed. The range of spectral phenomenology is illustrated from the JET tokamak using fast deuterium and helium beams. The helium observations are new. The atomic reactions concerned in the emission and their interplays are summarised. The state of cross-section data for the analysis is briefly assessed.

INTRODUCTION

Neutral beam associated spectroscopic measurements have become firmly established over the last ten years as a major diagnostic tool for tokamak fusion plasmas. For fast penetrating beams such as $^1H^0$, $^2D^0$, $^3He^0$ and $^4He^0$ at energies $\geq$ 25 keV/amu, diagnostic advance has been very fruitfully associated with the implementation of very powerful such sources for supplementary heating of plasmas **(1)**. Dedicated diagnostic beams of these types have since followed on. Proposals for the next international tokamak (ITER) include such H^0 and He^0 beams. By contrast, for the awkward environment of the plasma edge in large machines or for small diameter machines, the opportunities of using special beams such as $^7Li^0$ have long been realised **(2)**.

Beam related spectroscopic measurements arise from two sets of reactions. Using a deuterium beam for illustration, these are

$$D^0_{beam}(1s) + X^{+z_0}_{plasma} \rightarrow D^+_{beam} + X^{+z_0-1}_{plasma}(nl)$$

$$X^{+z_0-1}_{plasma}(nl) \rightarrow X^{+z_0-1}_{plasma}(n'l') + h\nu$$

in which charge exchange is the primary driving reaction and the emitted radiation gives information on the plasma ion $X^{+z_0}_{plasma}$. This is 'charge exchange spectroscopy' (CXS).
The other set is

$$D^0_{beam}(1s) + \left\{ \begin{matrix} X^{+z_0}_{plasma} \\ e \end{matrix} \right\} \rightarrow D^0_{beam}(nl) + \left\{ \begin{matrix} X^{+z_0}_{plasma} \\ e \end{matrix} \right\}$$

$$D^0_{beam}(nl) \rightarrow D^0_{beam}(n'l') + h\nu$$

in which beam excitation is the primary driving reaction and the emitted radiation characterises the beam atoms in the plasma environment. This is 'beam emission spectroscopy' (BES).

The advantages of such spectroscopy are :

(a) Inducing of emission associated with non-radiating fully ionised impurity species in the plasma core. This is the main reason for the relevance of CXS in high temperature fusion plasmas. The induced radiation is diagnostic of ion temperature **(3)**, plasma rotation **(4)** and impurity density. **(5)**.

(b) Localisation in space of the emission at the beam/viewing line intersection. For example, at JET a typical injector beam has a section $\sim$ 300 cm^2 at the plasma centre.

The optical viewing line aperture is $\sim$ 5 cm^2. For a 40 keV/amu $^2D^0$ beam, the radiative lifetime of the $n = 3$ shell is $\sim 10^{-8}$ sec and implies a decay length along the beam line of $\sim$ 2.5 cm. Therefore, for most purposes, the radiation is localisable and reflects the local reactions in the volume.

(c) Since the neutral beam atoms are traversing a magnetic field, the beam emission is in general resolvable into Zeeman, Paschen-Back **(2)** or motional Stark components depending on particle speeds and field strengths. **(6)**

(d) Discrimination of the beam/plasma emission from background and coincident radiation from the plasma edge is possible. Most precisely this is done by modulation of the beams and less well by pre-and post- beam measurement. In practice the difference in edge and central plasma feature widths often allows separation by constrained multi-gaussian fitting methods.

(e) Extended spectral regions over which CXS emission can be observed. This is especially true for fast beams because of the behaviour of charge exchange cross-sections to different quantum shells of the receiving ion and, in particular, allows easy visible wavelength observations.

The disadvantages are

(a) Attenuation of the beams. This necessitates careful calculation for quantitative studies. For example, in JET beam attenuation by a factor 100 can still gives measurable CXS spectral signals, but errors of $\sim$ 20% in the stopping cross-section are amplified to errors $\sim$ 100% in deduced impurity densities. It must also be noted that electron density measurements particularly near the edge of the plasma can be quite inaccurate.

(b) Mixed components in the beam. These may be fractional energy components in D^0 beams or metastable components in He^0 beams and add uncertainty to analysis.

(c) The initially formed states following charge exchange from the donor beam species are disturbed by further collisions with plasma ions and electrons before radiating in general.

For this and the previous reasons quite elaborate theoretical calculations, using many cross-sections, are necessary to allow signal interpretation. There is another complication. The beam/plasma interaction establishes a number of secondary populations which in turn act as the sources for further reactions. Also there are usually radiating populations at the edge of the plasma. Both sets of populations can emit at the same wavelengths as the sought CXS lines. The secondary populations are of some importance. To summarise, there are :

(a) Halo atoms - These are D^0_{plasma} atoms formed by reactions (1) with $X \equiv D$. They migrate in a random walk by futher CX reactions until ionised. Typically they are localised within $\sim$ 30cm of the beam itself.

(b) Plume ions - These are ions formed by reactions (1) They travel along field lines. Excited by electrons they can radiate before ionising in positions some distance from their point of formation (in JET, $\sim$ 40m for C^{+5} and $\sim$ 6m for He^{+1} at 5keV & 5.0^{13} cm^{-3}) **(7)**.

(c) The slowing ionised beam population. For example, for $^3He^0$ beams at 50 keV/amu in JET, the slowing down time of the fast $^3He^{+2}$ after double ionisation is $\sim$ .3 - .6 sec.

(d) Ions X^{+z0-1} and $X'^{+z'0-3}$ present at the periphery of the plasma. Note the spectral overlap of hydrogen-like and lithium-like emission.

It is to be noted that the population *(c)* is very similar to that of slowing alpha particles expected to be produced by D/T fusion **(8)**.

THE SPECTRAL PHENOMENOLOGY

In illustrating CXS and BES spectra from tokamaks, it must be noted that the particular geometric configuration of the machine and spectroscopic viewing lines influences strongly the relative importance of the various secondary populations. Equally the particular beam energies, concentrations of impurities, electron and plasma ion temperatures and densities determine the balance between the various atomic reactions. The data shown here are from the JET tokamak. The beam line configuration in JET is shown in plan view in figure 1, and has been described in detail elsewhere **(1)**.

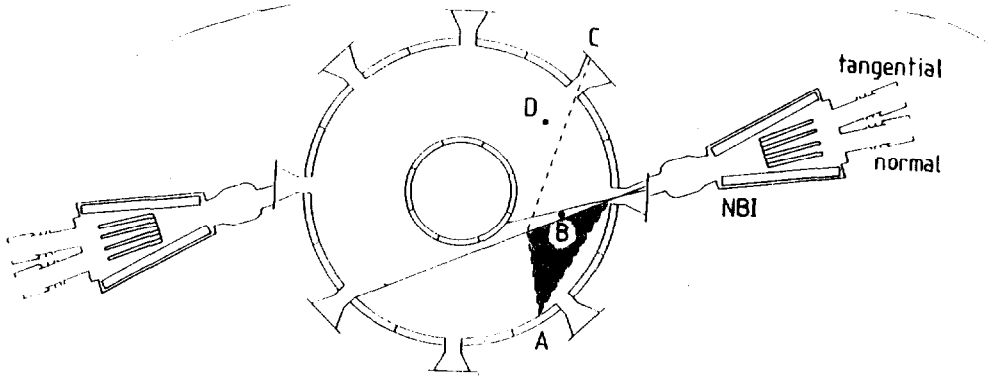

Fig. 1. Plan view of JET showing the two neutral beam injector assemblies organised as 'radial' and 'tangential' sets of four vertically arranged individual injectors. Spectral observations are allowed via a horizontal fan of viewing lines (A) ($\lambda \geq 4000$Å) and vertical lines at (B) ($\lambda \geq 3000$Å) and (D) ($\lambda \geq 4000$Å).

JET has been used to study beryllium as a limiter material and so provides a unique opportunity to observe beryllium CXS (9). Figure 2a shows the vicinity of 4685Å. The data was with deuterium beams at a primary energy of 40keV/amu. There are two CXS lines namely BeIV (n = 6-5) and BeIV (n = 8-6), distinctive because of their breadth. Each is a superposition of broad beam/plasma emission and edge emission. Figure 2b shows the same wavelength region but with modulated beams and appropriate subtractions.

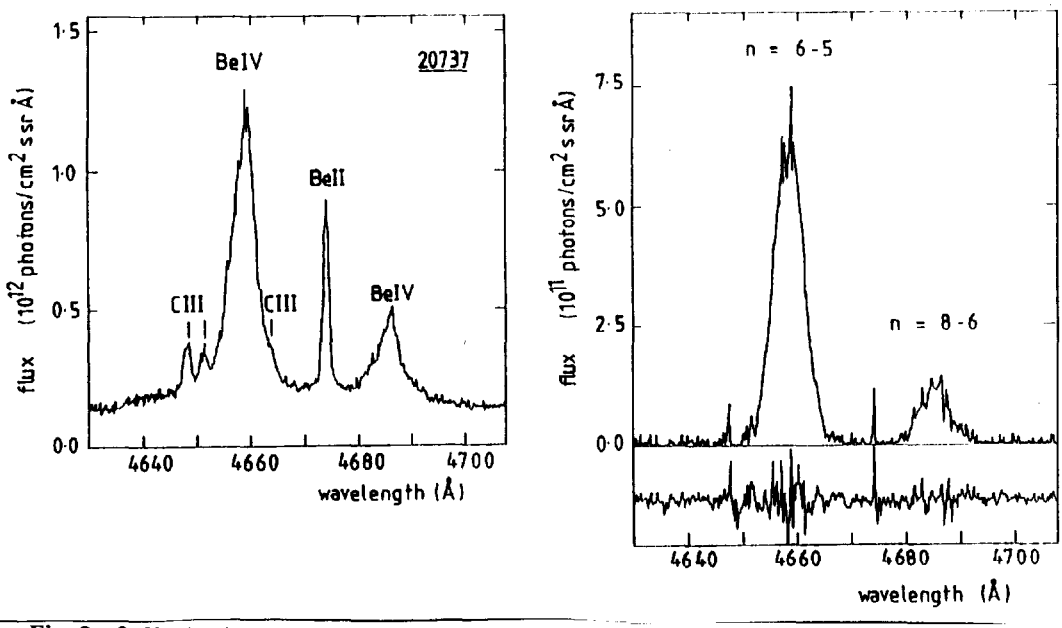

Fig. 2a & 2b. (a) Spectral observation through neutral D^0 beams showing edge (CIII, BeII and BeIV) emission and CXS (BeIV) emission. (b) The same spectral region with edge and background emission removed using modulated beam differences. The remaining features are pure gaussians at the same (central plasma) temperature.

The edge emission and bremsstrahlung background are effectively eliminated leaving pure CX features. Their ratio therefore challenges atomic reaction modelling of the effective emission coefficients. In general other hydrogen-like or lithium-like species of even nuclear charge can emit at the same wavelength (for example, HeII (n = 4-3) or CVI (n = 12-9)). Helium was not present in the pulses shown and carbon was low. The edge emission in BeII 4673.5Å is a narrow feature at $T_i \sim 20$ eV and provides a wavelength fiducial. The centrally emitted charge exchange lines generally show an apparent plasma rotation. The rotation is real but its magnitude is modified by the energy dependence of the driving charge exchange reaction cross-sections. For the faster moving light plasma ions in particular, the excursion of their relative speed to the beam atoms from the beam speed produces spectral shifts, width and intensity alterations **(10,11)**. These depend on the gradient and curvature of the reaction cross-section with relative speed. At $T_i = 20keV$, $E_{beam} = 40keV/amu$, $\Delta\lambda = 0.36Åred$, $\Delta T_i = 6keV$ for BeIV (n = 6-5). By contrast for the light ion He^{+2}, the temperature shift as observed in HeII (n=4-3) at 150° to the beam line is ΔT_i = 9.6 keV at T_i = 20 keV and $\Delta\lambda = 2.3Åblue$.

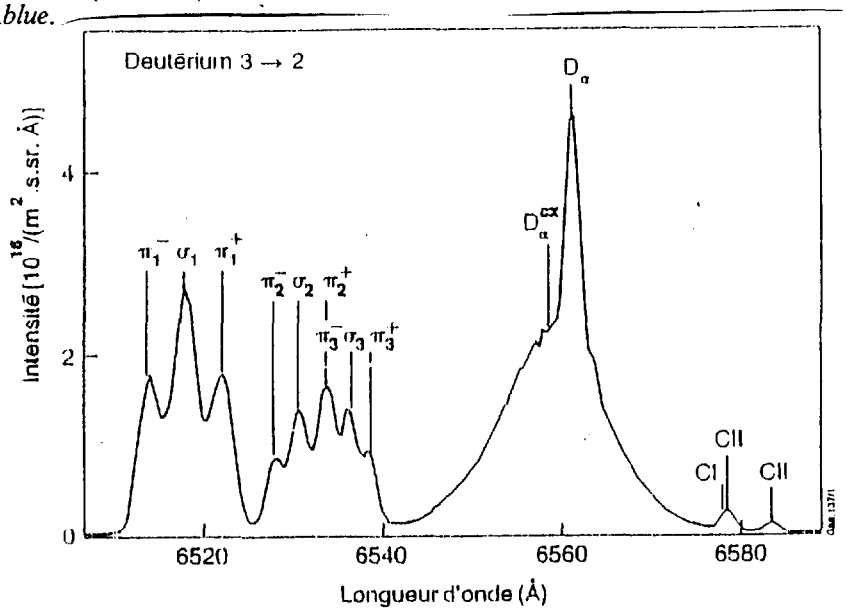

Fig. 3. Spectral observation through neutral D^0 beams in the vicinity of 6563Å showing edge D_α emission, CXS D_α emission, halo D_α emission and full, half and third energy beam D_α emission. Note the doppler shift and Stark separation of the latter.

Figure 3 shows the spectral vicinity of D_α at 6563Å The beam emission is the composite feature on the blue side, doppler shifted because of the inclination of the beam line to viewing line. This is very convenient for distinguishing beam emission. The feature is composed of full, half and third energy parts with different mean doppler shifts. D_α emission from the beams is resolved into Stark multiplets because of the $\underline{v}x\underline{B}$ electric field in the frame of the moving beam atoms. These initially suprising features **(6)** are becoming familiar to tokamak diagnosticians. Figure 3 also identifies the various π and σ components. The information on internal magnetic field strength and orientation contained in these features is of great interest for tokamak studies. **(12,13)**. On the other hand, the intensity of the features charts beam attenuation and collisionality through the plasma. Collisions with plasma and impurity ions are important here. Fluctuations in the beam intensity reflect density fluctuations in the plasma at least at frequencies accessible by the limits of signal integration time and on lengths scales set by radiative decay lengths **(14)**.

Figure 4 shows again the spectral vicinity of 4685Å. However this experiment was with $^3He^0$ beams at 50 keV/amu. Helium was the dominant minority species in the plasma and the feature at 4685Å is HeII (n = 4-3) primarily. It is probably the first illustration of CXS with helium beams. Initial estimates of the effective emission coefficient for this CXS line with

helium donor suggests that it is about 50% smaller than that with deuterium donor. On the other hand beam penetration is somewhat better so the overall impression is similar to that for deuterium beams. For other impurities such as beryllium and carbon, first impressions are that the CXS features are significantly weaker than for deuterium beams as indicated by our preliminary atomic cross-section data base for state-selective charge exchange capture with helium beams. Attention is drawn to the weak flat pedestal extending for 48 Å to the red side of 4685Å.

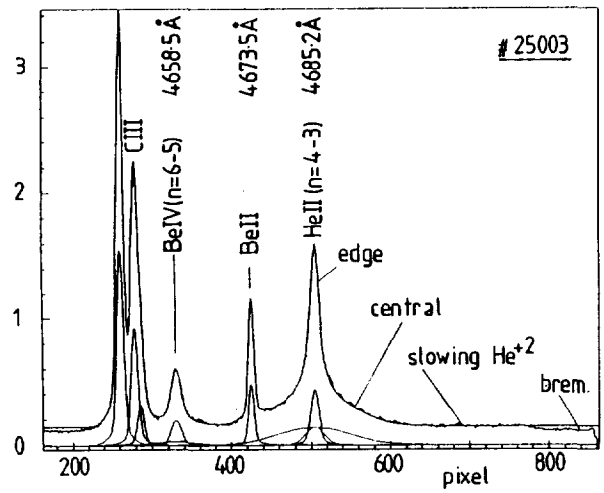

Fig. 4. Spectral observation through neutral $^3He^0$ beams showing edge (CIII, HeII, BeII and BeIV) emission, CXS (HeII) emission with the beams and emission from slowing He^{+2} (HeII).

This arises from a fast $^3He^{+2}$ population in the plasma generated by the helium beams. The wavelength extension of the feature corresponds to a 50kev/amu doppler shift and the feature is assumed to extend similarly to the blue. It is the first observation of a slowing alpha particle distribution.

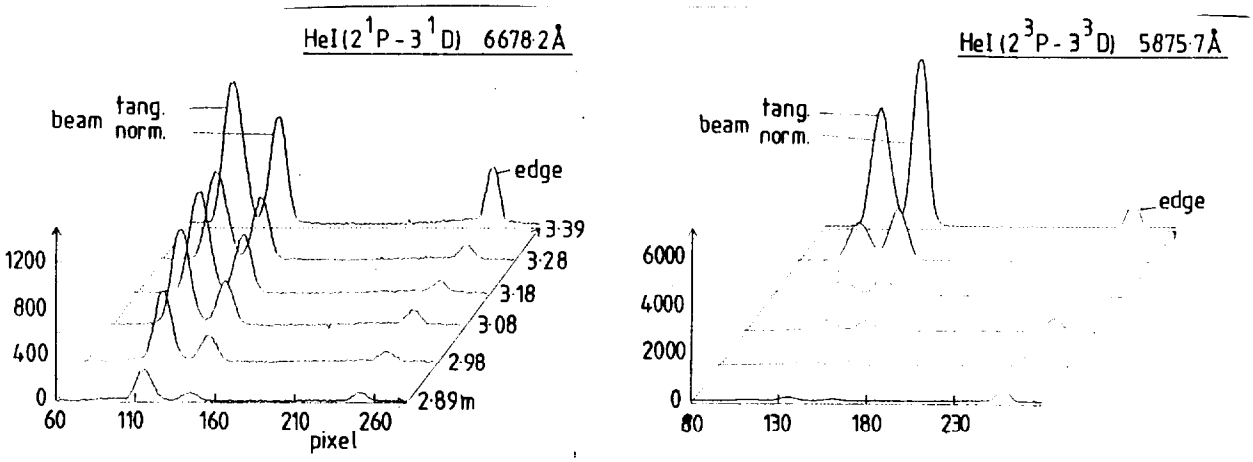

Fig. 5a & 5b. (a)Spectral observation through neutral $^3He^0$ beams in the vicinity of HeI (2p ^{1}P - 3d ^{1}D) at 6678 Å showing edge (HeI) emission and doppler shifted beam (HeI) emission. There are two beam lines contributing to the latter. (b) Spectral observation through neutral $^3He^0$ beams in the vicinity of HeI (2p ^{3}P - 3d ^{3}D) at 5876 Å showing edge (HeI) emission and doppler shifted beam (HeI) emission. There are two beam lines contributing to the latter.

Decay of the feature on time scales ~ 0.3 sec. after beam switch off indicates that the emission is not being detected by the helium beam as a CXS donor on the fast population but rather is associated with thermal deuterium CX at the hydrogen rich edge 'X-point' regions of the plasma. In JET there is deuterium gas introduction at these points to provide a protective cooling mantle for the beryllium target plates. This point is not yet fully demonstrated.
Finally figures 5a and 5b show the spectral vicinities of HeI ($2p^1P$ - $3d\ ^1D$) at 6678.2Å and of HeI ($2p^3P$ - $3d\ ^3D$) at 5875.7Å respecively. HeI edge emission is observed at the nominal wavelengths. The double feature in each case to shorter wavelengths is the helium beam emission. The viewing line intersects 'tangential' and 'normal' neutral beam lines with different inclinations. The strength of the triplet side spectrum in the beam is of note. The metastable content of helium beams formed by He^+/He neutralisation has been the subject of some discussion **(15,16)**. It is expected to be < 7%. At a beam particle energy of 50kev/amu penetrating in a plasma of Z_{eff} = 1, the $2\ ^3S$ stopping length is ~ 50cm. compared with ~ 1m for $1\ ^1S$ at 5keV and 5.0^{13} cm^{-3}. The initial entrant metastable fraction, its destruction and the regeneration of the metastable population in the plasma is important for diagnostic studies. Evidently with such observations a complete CXS and perhaps BES is possible with helium beams as the donor.

ATOMIC REACTIONS AND CROSS-SECTIONS - HYDROGEN BEAMS

The atomic reactions of concern are firstly those responsible for beam stopping. At low density, these are direct losses from the beam atoms in their ground state. For $^2D^0$ beams it is given by the sum of the reactions (1) and the ionising reactions

$$D^0_{beam}(1s) + \left\{ \begin{matrix} X^{+z_0}_{plasma} \\ e \end{matrix} \right\} \rightarrow D^+ + \left\{ \begin{matrix} X^{+z_0}_{plasma} \\ e \end{matrix} \right\} + e$$

Above 20 keV/amu ion collisions dominate electron collisions. In the large tokamaks, high ion temperatures, $T_i \leq$ 30keV, are encountered, so proper displaced Maxwell averages must be used in the equations. Cross-section data for D^+ and He^{+2} is good at all energies (10% accuracy at least is required). For the other light nuclei, the high energy region E $\geq$ 100keV/amu is good but ionisation cross-sections are poorly known below 80kev/amu. Although the stopping then is dominated by the charge exchange cross-sections, it is still difficult to be certain of 10% accuracy for ions of $z_0 \geq 3$

At high densities, stepwise losses via excited states become relevant, that is collisional-radiative rates are required. So excitation cross-sections matter. These excitation processes of course are the equations (2) involved in formation of the beam emission spectrum. The situation for excitation cross-sections is much less satisfactory especially for $z \geq 2$. For ion collisions in the relevant regions 10 kev/amu $\leq E \leq$ 70 keV/amu, scaling rules of the $\frac{\sigma}{z} / \frac{E}{z}$ type (see **(17)** for a discussion) break down. Also little experimental data is available at these energies for $z_0 \geq 3$. This is the regime where the elaborate close-coupled atomic orbital calculations are of great assistance **(18)**.
Figure 6 shows the new data for He^{+2}/H by Fritsch et al. **(19)** contrasted with older data. The oscillations are of note and influence modelling of higher density beam stopping and beam emission spectroscopy. Large scale population calculations making use of such data establish tabulations of beam stopping coefficients and effective emission coefficients of all spectrum lines of deuterium for all beam energies and plasma conditions. Figure 7 contrasts theory and experiment using multichord observations of D_α at JET. The primary impurity was carbon and Z_{eff} was ~ 3. Evidently this area of BES is progressing, justifying the cross-secion efforts.

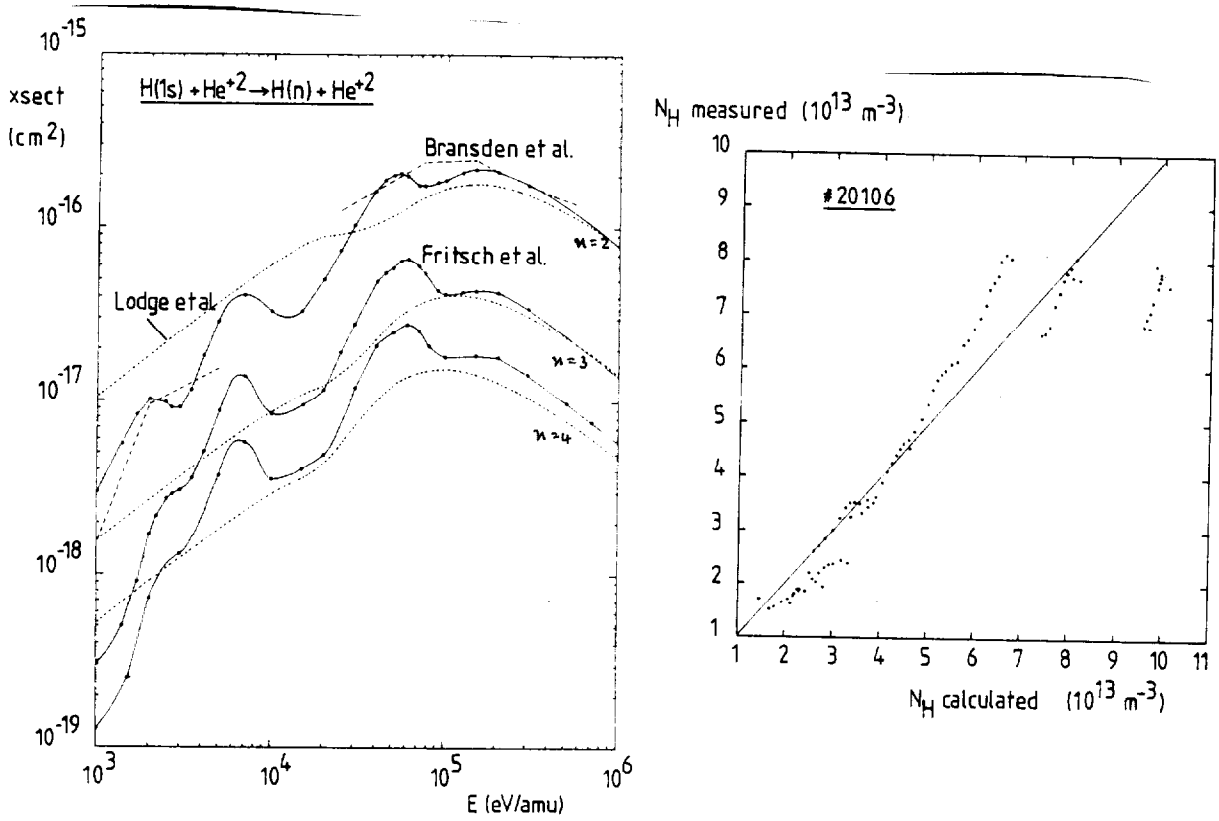

Fig. 6 & 7. (6) Comparison of *H(1s)* excitation cross- sections due to He^{+2} impact. (7) Calculated and measured density of the primary energy fraction of the neutral deuterium beam in the plasma. The measured values are deduced from D_α.

CXS of impurities in tokamaks requires firstly state selective charge exchange cross-sections for the fully ionised ions of H, He and the first period atoms *Be – Ne*. Then, less routine, is CXS of heavier species such as iron, and also of partially stripped recombining ions particularly with helium-like or neon-like configurations. Since observations concentrate on the visible spectral region, capture cross-sections to *n*-shells with subdominant $n > z_0^{3/4}$ must be known and indeed the fractions into *l*-substates. Fields and ion collisions partially redistribute the *l* populations. This is very testing both for experiment and theory. The energy region 5 keV/amu to 200 keV/amu is required which spans from the molecular to the high energy regimes. Elaborate calculations and sophisticated experiments have contributed enormously to the available database in response to the fusion needs. In illustration, figure 8 reviews the state selective data for He^{+2}/H **(11)**. Extensive collisional-radiative calculations of various types such as l-mixing cascade, bundle-nl and bundle-n **(20)** convert such data to the derived effective emission coefficients, mapped over plasma parameters, for the particular CXS lines used for experiment analysis. Improvements which take account of the secondary populations present further difficult demands on fundamental cross-section calculations. For example, the decreasing charge exchange capture to a high excited *n*-shell at lower energies means that CX from excited states of fractional energy beam atoms or from halo atoms have an opportunity to contribute. The role of excited state donors increases down to thermal edge features where it is completely dominant **(21)**. Extensive calculations have been carried out extending the state selective CX database from excited donors over the whole collision energy range. Clearly such influences are hard to distinguish from structure in the ground state direct capture cross-sections shown in figure 8 and both must be accorded appropriate attention in the atomic modelling.

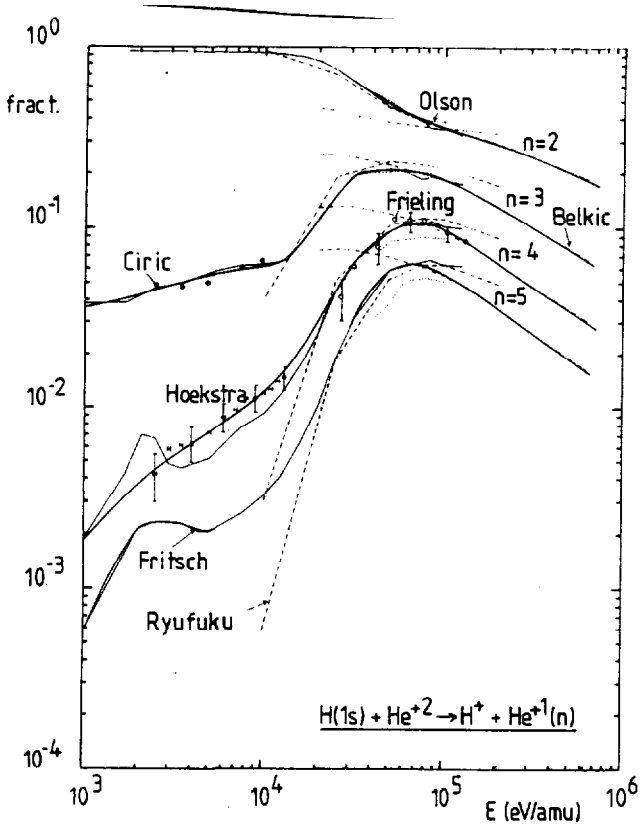

Fig. 8. New measurements and assessment of the partial capture cross-sections into n-shells in He^{+2}/H collisions.

ATOMIC REACTIONS AND CROSS-SECTIONS - HELIUM BEAMS

Helium beam stopping is more complicated than that of hydrogen. In addition to the single electron loss processes from the ground state as in equations (1) and (3), there are two electron loss processes of double ionisation, double charge transfer and transfer ionisation.

$$He^{0}_{beam}(1s^2\ ^1S) + X^{+z_0}_{plasma} \rightarrow He^{+2} + X^{+z_0}_{plasma} + e + e$$

$$He^{0}_{beam}(1s^2\ ^1S) + X^{+z_0}_{plasma} \rightarrow He^{+2} + X^{+z_0-2}_{plasma}$$

$$He^{0}_{beam}(1s^2\ ^1S) + X^{+z_0}_{plasma} \rightarrow He^{+2} + X^{+z_0-1}_{plasma} + e$$

For He^{+2}, the double charge transfer is resonant. Figure 10 shows the various stopping cross-sections as used in the JET database for Be^{+4}. Note that at the 10% level of accuracy at 50 kev/amu all the processes need to be considered. For single CX there are no experiments, single ionisation below 100 keV/amu, transfer-double ionisation below 100keV/amu and double charge transfer are speculative. Comprehensive experimental data is available only for H^+ and He^{+2} and partial experimental data for Li^{+3} **(22)**. At higher density and with a metastable content of the beam at source, the $2\ ^1S$ and $2\ ^3S$ metastables must be incorporated in the modelling of stopping since they are most influential on the stepwise collisional-radiative pathways. For BES, evidently transitions from the n = 3 to 2 levels on both the singlet and triplet side are the most immediately useful. The most interesting properties however are in the n = 4 shell. The $\underline{v}x\underline{B}$ motional Stark field mixes the $4f^1F$, $4d^1D$, $4p^1P$ progressively as the electric field increases up to 100 kV/cm. The resulting forbidden line positions are shown in figure 10. Unfortunately, unlike hydrogen the branching ratio $(1s^2\ ^1S - 1s4p\ ^1P)/(1s2s\ ^1S - 1s4p\ ^1P)$ is $\sim$ 34/1 . With the mixing, transitions from the $4p$ to the ground act as a drain on the populations of the $n = 4$ levels and so the visible wavelength features must be very weak.

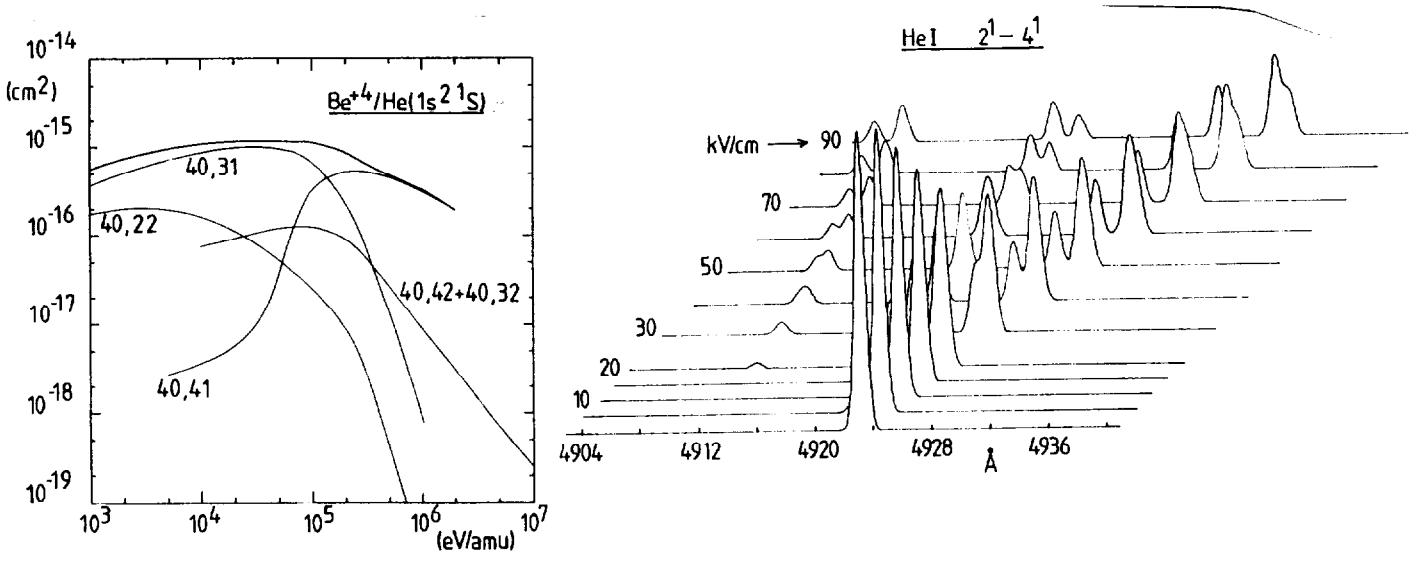

Fig. 9 & 10. (9) Stopping cross-sections for $He(1\,{}^1S)$ in collision with Be^{+4} at zero density. (10) Theoretical Stark patterns for HeI (n=2-4) singlets with increasing electric field strength viewed othogonal to the electric field.

These features have not yet been observed on JET at integration times of 1 sec. although blue enhancement of detectors may allow this at a later stage.
Population of the triplet side in the plasma from the ground state is difficult, since spin changing collision cross-sections by electrons become very small at $T_e \geq 2$ keV. Population is more likely through spin system breakdown of 4 ^{1}F and 4 ^{3}F under the Breit interaction. Clearly more observations of helium beams are required before the helium BES is fully understood and the opportunities for diagnostic application explored. Turning to CXS with helium beams, the data base of state selective charge exchange cross-sections to subdominant n-shells in the 10 keV/amu - 100 kev/amu range appears to be almost non-existent except with H^+ (see Hoekstra et al. - this meeting) although the situation is better at higher energies. A transfer database from deuterium is at present in use at JET, based on overbarrier model considerations. Its validity remains uncertain although initial comparisons with observations are encouraging. The role of the helium metastables as donors remains ambiguous. For $C^{+5}(n=8)$ theoretical estimates suggest that the 2 ^{3}S CX contribution is less than that from 1 ^{1}S. Evidently considerably more effort is required to bring CXS with helium beams to the same state as that with hydrogen beams. It is likely that helium beams in the 30 keV/amu - 50 kev/amu will be used quite extensively in fusion plasma studies and so may justify such effort.

ATOMIC REACTIONS AND CROSS-SECTIONS - LITHIUM BEAMS

Use of low energy lithium beams, $E \sim 10$ keV/amu parallels that of the hydrogen and helium fast beams. The short ionisation lengths of Li^0 in a plasma ($\sim$ 10 cm decay length for 60 keV beams at density $\sim 2.0^{13}$ cm^{-3}) makes it most valuable as an edge probe. The decay of the resonance line radiation at 6707.8Å is described with multi-level ($n \leq 3$ typically) collisional-radiative models.

Measurements along the decay path of the beam allow reconstruction of the density profile **(23)**. Electron and ion collisions are both involved. Likewise CXS with Li^0 as the donor has been carried out (for example on C^{+6} and C^{+5} as receiver **(24)**). After spectral separation of the π component of the resonance line (Pashen-Back separations of π and σ components are typically $\sim$ 0.2Å) measurement of its polarisation angle has been successfully used to obtain the internal magnetic field orientation and hence the current distribution in small tokamaks **(2)**.

CONCLUSIONS

The paper has sought to show some of the highlights of charge exchange spectroscopy and beam emission spectroscopy in tokamak plasmas. Extensive modelling of the collisional-radiative type is required for full exploitation of these active diagnostics. The enormous international effort on fundamental ion/atom collision cross-sections has given credibility to this, such that increasingly precise and subtle deductions are pursued. All modern large tokamak enterprises now depend on their CXS and BES diagnostics.

REFERENCES

(1) A Boileau, M von Hellermann, L D Horton & H P Summers (1989) Plasma Phys.and Contr. Fusion 31, 779.
(2) K McCormick (1986) Proceedings of 'Basic and Advanced Diagnostic Techniques for Fusion Plasmas', Varenna, p635.
(3) R J Fonck, R J Goldston, R Kaita & D E Post (1983) Appl. Phys. Lett. 42, 239.
(4) R J Groebner, N H Brooks, K H Burrell & L Rottler (1983) Appl. Phys. Lett. 43, 920.
(5) R C Isler (1981) Phys. Rev. A 24, 2701.
(6) A Boileau, M von Hellermann, W Mandl, H P Summers, H Weisen & A Zinoviev (1989) J. Phys. B 22, L145.
(7) R J Fonck, D S Darrow & K P Jaehnig (1984) Phys. Rev. A 29, 3288.
(8) D E Post (1981) J. Fusion Energy 1, 129.
(9) H P Summers, W J Dickson, A Boileau, P G Burke, B Denne-Hinnov, W Fritsch, R Giannella, N C Hawkes, M von Hellermann, W Mandl, N J Peacock, R Reid, M F Stamp & P R Thomas (1991) Plasma Phys.and Contr. Fusion - in press.
(10) M von Hellermann, W Mandl, H P Summers, H Weisen, A Boileau, P D Morgan, H Morsi, R Koenig, M F Stamp & R Wolf (1990) Re. Sci. Intrum. 61, 3479.
(11) M von Hellermann, W Mandl, H P Summers, A Boileau, R Hoekstra, F J de Heer & J Frieling (1991) Plasma Phys. and Contr. Fusion - in press.
(12) C Challis, M von Hellermann, B Keegan, R Konig, W Mandl, J O'Rourke, R Wolf & W Zwingmann (1991) '18th European Physical Society Conf. on Controlled Fusion & Plasma Physics, Berlin. JET-P(91)08.
(13) D Wroblewski, K H Burrell, L L Lao, P Politzer & W P West (1990) Rev. Sci. Instrum. 61,3552.
(14) S F Paul & R J Fonck (1990) Rev. Sci. Instrum. 61,3496.
(15) K Tobita, T Itoh, A Sakasai, Y Kusama, Y Ohara, Y Tsukahara, M Nemoto, Y Kawano, H Kubo, H Takeuchi & T Sugie (1990) Plasma Phys. and Contr. Fusion 32, 429.
(16) R S Hemsworth (1991) - private communication
(17) W Fritsch & K-H Schartner (1987) Physics Letters 126, 17.
(18) W Fritsch & C D Lin (1991) Physics Reports 202, 1.
(19) W Fritsch, R Shingal & C D Lin (1991) Phys. Rev. A - in press.
(20) J Spence & H P Summers (1986) J. Phys. B 19, 3749.
(21) M Mattioli, N J Peacock, H P Summers, B Denne & N C Hawkes (1989) Phys. Rev. A 40, 3886.
(22) M B Shah & H B Gilbody (1985) J. Phys. B 18, 899.
(23) F Aumayr, M Schneider, E Unterreiter & H. Winter (1991) - .
(24) R P Schorn, E Hintz, D Rusbuldt, F Aumayr, M Schneider, E Unterreiter & H Winter (1991) J. Phys. B 91, - .

Appendix I

THE JET TEAM

JET Joint Undertaking, Abingdon, Oxon, OX14 3EA, U.K.

J.M. Adams[1], H. Altmann, A. Andersen[14], P. Andrew[18], M. Angelone[29], S.A. Arshad, W. Bailey, P. Ballantyne, B. Balet, P. Barabaschi, R. Barnsley[2], M. Baronian, D.V. Bartlett, A.C. Bell, I. Benfatto[5], G. Benali, H. Bergsaker[11], P. Bertoldi, E. Bertolini, V. Bhatnagar, A.J. Bickley, H. Bindslev[14], T. Bonicelli, S.J. Booth, G. Bosia, M. Botman, D. Boucher, P. Boucquey, P. Breger, H. Brelen, H. Brinkschulte, T. Brown, M. Brusati, T. Budd, M. Bures, T. Businaro, P. Butcher, H. Buttgereit, C. Caldwell-Nichols, D.J. Campbell, P. Card, G. Celentano, C.D. Challis, A.V.Chankin[23], D. Chiron, J. Christiansen, C. Christodoulopoulos, P. Chuilon, R. Claesen, S. Clement, E. Clipsham, J.P. Coad, M. Comiskey[4], S. Conroy, M. Cooke, S. Cooper, J.G. Cordey, W. Core, G. Corrigan, S. Corti, A.E. Costley, G. Cottrell, M. Cox[7], P. Cripwell, H. de Blank[15], H. de Esch, L. de Kock, E. Deksnis, G.B. Denne-Hinnov, G. Deschamps, K.J. Dietz, S.L. Dmitrenko, J. Dobbing, N. Dolgetta, S.E. Dorling, P.G. Doyle, D.F. Düchs, H. Duquenoy, A. Edwards, J. Ehrenberg, A. Ekedahl, T. Elevant[11], S.K. Erents[7], L.G. Eriksson, H. Fajemirokun[12], H. Falter, D. Flory, J. Freiling[15], C. Froger, P. Froissard, K. Fullard, M. Gadeberg, A. Galetsas, D. Gambier, M. Garribba, P. Gaze, R. Giannella, A. Gibson, R.D. Gill, A. Girard, A. Gondhalekar, C. Gormezano, N.A. Gottardi, C. Gowers, B.J. Green, R. Haange, G Haas, A. Haigh, G. Hammett[6], C.J. Hancock, P.J. Harbour, N.C. Hawkes[7], P. Haynes[7], J.L. Hemmerich, T. Hender[7], F.B. Herzog, R.F. Herzog, J. Hoekzema, J. How, M. Huart, L Hughes, T.P. Hughes[4], M. Hugon, M. Huguet, A. Hwang[7], B. Ingram, M. Irving, J. Jacquinot, H. Jaeckel, J.F. Jaeger, G. Janeschitz[13], S. Jankowicz[22], O.N. Jarvis, F. Jensen, E.M. Jones, L.P.D.F. Jones, T.T.C. Jones, J-F. Junger, E. Junique, A. Kaye, B.E. Keen, M. Keilhacker, G.J. Kelly, W. Kerner, R. Konig, A. Konstantellos, M. Kovanen[20], G. Kramer[15], P. Kupschus, R. Lässer, J.R. Last, B. Laundy, L. Lauro-Taroni, K. Lawson[7], M. Lennholm, A. Loarte, R. Lobel, P. Lomas, M. Loughlin, C. Lowry, B. Macklin, G. Maddison[7], G. Magyar, W. Mandl[13], V. Marchese, F. Marcus, J. Mart, E. Martin, R. Martin-Solis[8], P. Massmann, G. McCracken[7], P. Meriguet, P. Miele, S.F. Mills, P. Millward, R. Mohanti[17], P.L. Mondino, A. Montvai[3], S. Moriyama[28], P. Morgan, H. Morsi, G. Murphy, M. Mynarends, R. Myrnäs[16], C. Nardone, F. Nave[21], G. Newbert, M. Newman, P. Nielsen, P. Noll, W. Obert, D. O'Brien, J. O'Rourke, R. Ostrom, M. Ottaviani, M. Pain, F. Paoletti, S. Papastergiou, D. Pasini, A. Peacock, N. Peacock[7], D. Pearson[12], R. Pepe de Silva, G. Perinic, C. Perry, M. Pick, R. Pitts[7], J. Plancoulaine, J-P. Poffé, F. Porcelli, L. Porte[19], R. Prentice, S. Puppin, S. Putvinsko[23], G. Radford[9], T. Raimondi, M.C. Ramos de Andrade, P-H. Rebut, R. Reichle, E. Righi, F. Rimini, D. Robinson[7], A. Rolfe, R.T. Ross, L. Rossi, R. Russ, P. Rutter, H.C. Sack, G. Sadler, G. Saibene, J.L. Salanave, G. Sanazzaro, A. Santagiustina, R. Sartori, C. Sborchia, P. Schild, M. Schmid, G. Schmidt[6], B. Schunke, S.M. Scott, A. Sibley, R. Simonini, A.C.C. Sips, P. Smeulders, R. Stankiewicz[27], M. Stamp, P. Stangeby[18], D.F. Start, C.A. Steed, D. Stork, P.E. Stott, T.E. Stringer, P. Stubberfield, D. Summers, H. Summers[19], L. Svensson, J.A. Tagle[21], A. Tanga, A. Taroni, A. Tesini, P.R. Thomas, E. Thompson, K. Thomsen, J.M. Todd, P. Trevalion, B. Tubbing, F. Tibone, E. Usselmann, H. van der Beken, G. Vlases, M. von Hellermann, T. Wade, C. Walker, R. Walton[6], D. Ward, M.L. Watkins, M.J. Watson, S. Weber[10], J. Wesson, T.J. Wijnands, J. Wilks, D. Wilson, T. Winkel, R. Wolf, B. Wolle[24], D. Wong, C. Woodward, Y. Wu[25], M. Wykes, I.D. Young, L. Zannelli, Y. Zhu[26], W. Zwingmann.

PERMANENT ADDRESSES

1. UKAEA, Harwell, Didcot, Oxon, UK.
2. University of Leicester, Leicester, UK.
3. Central Research Institute for Physics, Academy of Sciences, Budapest, Hungary.
4. University of Essex, Colchester, UK.
5. ENEA-CNR, Padova, Italy.
6. Princeton Plasma Physics Laboratory, New Jersey, USA.
7. UKAEA Culham Laboratory, Abingdon, Oxon, UK.
8. Universidad Complutense de Madrid, Spain.
9. Institute of Mathematics, University of Oxford, UK.
10. Freien Universität, Berlin, F.R.G.
11. Swedish Energy Research Commission, S-10072 Stockholm, Sweden.
12. Imperial College of Science and Technology, University of London, UK.
13. Max Planck Institut für Plasmaphysik, Garching bei München, FRG.
14. Risø National Laboratory, Denmark.
15. FOM Instituut voor Plasmafysica, 3430 Be Nieuwegein, The Netherlands.
16. University of Lund, Sweden.
17. North Carolina State University, Raleigh, NC, USA
18. Institute for Aerospace Studies, University of Toronto, Downsview, Ontario, Canada.
19. University of Strathclyde, 107 Rottenrow, Glasgow, UK.
20. Nuclear Engineering Laboratory, Lapeenranta University, Finland.
21. CIEMAT, Madrid, Spain.
22. Institute for Nuclear Studies, Otwock-Swierk, Poland.
23. Kurchatov Institute of Atomic Energy, Moscow, USSR
24. University of Heidelberg, Heidelberg, FRG.
25. Institute for Mechanics, Academia Sinica, Beijing, P.R. China.
26. Southwestern University of Physics, Leshan, P.R. China.
27. RCC Cyfronet, Otwock Swierk, Poland.
28. JAERI, Naka Fusion Research Establishment, Ibaraki, Japan.
29. ENEA, Frascati, Italy.

At 1st June 1991